KNOWLEDGE DISCOVERY IN CONCEPTUAL DESIGN OF SPACE PLANES USING MULTI-OBJECTIVE OPTIMIZATION AND DATA MINING

Takahiro Fujikawa*
*The University of Tokyo

Keywords: multidisciplinary design optimization, TSTO space planes, multi-objective optimization, data mining, future space transportation

Abstract

In this paper, multi-objective, multidisciplinary design optimization is conducted on the first stage vehicle of a horizontal takeoff and landing two-stage-to-orbit (TSTO) space plane with rocket-based combined cycle (RBCC) engines. A design optimization framework considering the interdependence among analysis disciplines (i.e., flight trajectories, propulsion, vehicle geometries, and aerodynamics) is constructed, and the vehicle design and the trajectory prior to the separation of the second stage vehicle are optimized simultaneously aiming to maximize the final velocity, minimize the gross mass of the first stage vehicle, and minimize the takeoff velocity. By solving this multi-objective optimization problem using a newly developed method, a set of pareto optimal solutions with a good spread is obtained. In addition to the discussions on some representative solutions, knowledge discovery in all the obtained solutions is performed via data mining techniques.

1 Introduction

Huge improvement to space transportation systems must be achieved in terms of cost efficiency, operability, and reliability in order to make the space industry profitable. Reusable launch vehicles or space planes with airbreathing engines are expected to satisfy this requirement and have been studied for years. Japan Aerospace Exploration Agency (JAXA) is currently working to

design a 'reference system' of reusable launch vehicles for the future space transportation [1, 2]. This is a challenging task due to the presence of complex interdependence among its design disciplines (e.g., flight trajectories, propulsion, vehicle geometries, aerodynamics, and structures). One of the approaches for this kind of multidisciplinary optimization (MDO) problem is to formulate it as an augmented trajectory optimization problem [3, 4, 5] and to subsequently solve it using direct trajectory optimization techniques [6]. While this framework enables simultaneous optimization of the vehicle and the trajectory efficiently, it has only been applicable to problems with a single design objective. It is difficult to establish a single design criterion in the early stage of design studies.

In other areas of optimal design methodologies, on the other hand, more than one objective function is frequently considered. In multiobjective optimization, evolutionary algorithms (EAs) are usually employed to numerically find a set of pareto optimal solutions. After the solution, it is possible to extract useful knowledge on the optimally designed system via applying data mining techniques to the obtained solutions. Whereas these procedures are successfully used mainly in aerodynamic design problems [7, 8], they are not as well suited to trajectory design problems because multi-objective EAs have some weaknesses in parameter interactions and equality constraints that are inherent in trajectory design problems [9, 10].

In order to overcome this difficulty, the author has developed an algorithm for obtaining uniformly spread pareto optimal solutions of multiobjective trajectory optimization problems [11]. In this paper, this method is applied to a conceptual design study of the first stage vehicle (booster) of a horizontal takeoff and landing TSTO space plane with RBCC engines. Three design objectives are considered together, and the booster design and the trajectory prior to the separation of the second stage vehicle (orbiter) are optimized simultaneously. By applying data mining techniques to the obtained set of pareto optimal solutions, correlation of objective functions and design variables (including static and dynamic ones) is revealed. The result is helpful not only for establishing design guidelines for the 'reference system' of space planes but also for future design studies using higher fidelity numerical models.

The remainder of this paper is organized as follows: Section 2 describes an MDO framework and numerical models therein. In Section 3, the multi-objective MDO problem is formulated, and the employed optimization methodology is briefly explained. The obtained set of pareto optimal solutions is shown, and knowledge discovery is performed in Section 4. Finally, Section 5 summarizes this paper and gives some future work.

2 MDO Framework and Numerical Models

In this paper, an MDO framework for the booster of a TSTO system consists of analysis disciplines of propulsion system, vehicle design and dry mass, aerodynamic forces, and the flight trajectory, as outlined in Fig. 1. Design variables include trajectory design parameters \mathbf{z}_t , vehicle design parameters \mathbf{z}_{v} , and auxiliary parameters \mathbf{z}_{a} . \mathbf{z}_{v} and \mathbf{z}_{a} are composed of static parameters enumerated in Table. 1. Broadly speaking, \mathbf{z}_t specifies the time history of flight conditions and will be further described in Section 3. A numerical model in each discipline calculates output values from the design variables and/or input values from other disciplines. As a consequence of these interactions, objective values and constraint values are produced. In the analyses of propulsion system and aerodynamic forces, surrogate models are utilized rather than numerical models themselves so as to reduce the computational burden and to enhance the numerical stability of optimization computation.

2.1 Propulsion System

The propulsion system installed in the booster is an ethanol-fueled RBCC engine which has been researched and developed in JAXA [12]. The RBCC engine combines the rocket and the airbreathing engine (ram/scramjet) into a unified engine cycle, leading to superior performance to conventional rockets. The engine is operated by successively switching three modes: ejector-jet (the rocket chamber pressure = 6 MPa), ramjet (0.6 MPa), and scramjet + rocket (6 MPa). Performance data of RBCC engines calculated by an analytic method [13] is provided by JAXA. For the following input conditions: Mach number M, angle of attack α , and dynamic pressure q; the following three output datasets are available: net

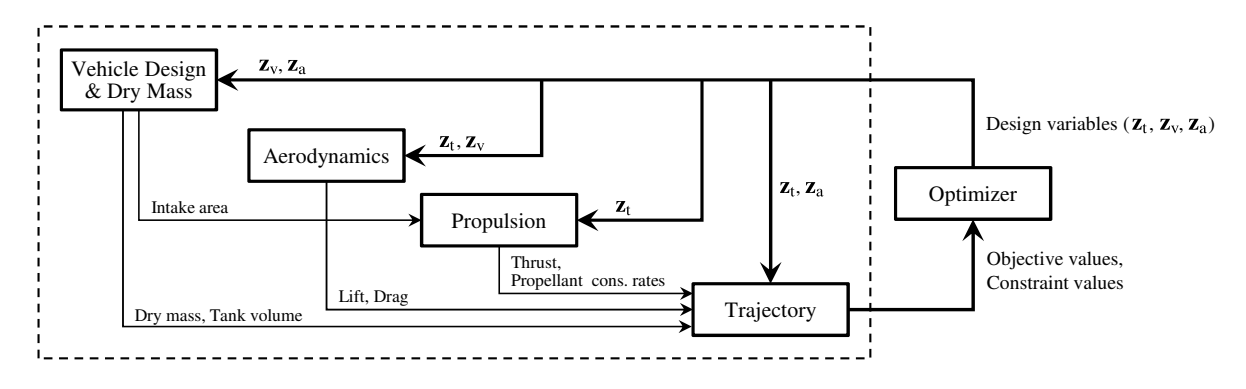


Fig. 1 An MDO framework for the booster of a TSTO system.

Parameter		Description		Associated constraints	
\mathbf{z}_{v}	$b_{ m ll}$	Length of the fuselage		$30 \le b_{\rm ll} \le 60$	
	$b_{ m w}$	Width of the fuselage	m	$0.1 \le b_{ m w}/b_{ m ll} \le 0.4$	
	$b_{ m hu}$	Height of the fuselage	m	$0.02 \le b_{\rm hu}/b_{\rm ll} \le 0.05$	
	$b_{ m wed}$	Inclination of the lower surface of the fuselage nose	deg	$0.0 \le b_{\mathrm{wed}} \le 10$	
	$b_{ m ln}$	Length of the fuselage nose	m	$0.1 \le b_{ m ln}/b_{ m ll} \le 0.4$	
	$b_{ m wn}$	Width of the fuselage nose	m	$0.4 \le b_{\mathrm{wn}}/b_{\mathrm{w}} \le 0.8$	
	$w_{\rm f}$	Front position of the exposed wing	m	$0.5 \le w_{\rm f}/b_{\rm ll} \le 0.8$	
	$w_{\rm chrd}$	Root chord length of the exposed wing	m	$0.1 \le w_{\text{chrd}}/b_{\text{ll}} \le 0.5$, $(w_{\text{f}} + w_{\text{chrd}})/b_{\text{ll}} \le 0.95$	
	w_{Λ}	Sweepback of the wing leading edge	deg	$45 \le w_{\Lambda} \le 70$	
	$t_{ m lof}$	Front position of the LO2 tank	m	$0.0 \le t_{ m lof}$	
	$t_{ m lor}$	Rear position of the LO2 tank	m	$t_{ m lof} \le t_{ m lor}$	
	$t_{\rm eaf}$	Front position of the ethanol tank	m	$t_{\rm lor} + 0.02b_{ m ll} \le t_{ m eaf}$	
	$t_{\rm ear}$	Rear position of the ethanol tank	m	$t_{\mathrm{eaf}} \leq t_{\mathrm{ear}} \leq b_{\mathrm{ll}}$	
	e_1	Length of the engines	m	$0.5 \le e_{\rm l}/b_{\rm ll} \le 0.8$	
	e_{w}	Width of the aggregate engines	m	$0.1 \le e_{\rm w}/b_{\rm w} \le 1.0$	
\mathbf{z}_{a}	aa_{\max}	Maximum axial acceleration	_	$aa_{\text{max}} \leq 3.0$	
	lf_{max}	Maximum load factor	_	$lf_{\max} \leq 1.5$	
	q_{max}	Maximum dynamic pressure	kPa	$q_{\text{max}} \le 50$	
	th_{\max}	Maximum thrust	N	_	
		Tentative gross mass of the booster	kg	Agreement to actual gross mass m_g^{boo}	
	$m_{ m gt}^{ m boo} \ m_{ m dryt}^{ m boo}$	Tentative dry mass of the booster	kg	Agreement to actual dry mass $m_{\text{dry}}^{\text{boo}}$	

Table 1 Vehicle design parameters \mathbf{z}_{v} and auxiliary parameters \mathbf{z}_{a} in the MDO problem.

thrust T, mass flow rate of ethanol fuel $G_{\rm ea}$, and mass flow rate of liquid oxygen (LO2) $G_{\rm lo}$.

In the MDO framework, thrust and propellant consumption rates are calculated from the engine operating mode, flight conditions, and the intake area of engines. This is done by evaluating kriging surrogate models [14] of the engine data assuming that thrust and propellant consumption rates are proportional to the intake area. The detailed engine design and the interaction between propulsion and airframe are not handled in this paper.

2.2 Vehicle Design and Dry Mass

The basic configuration of the booster is based on that of NASA's X-43A. RBCC engines are installed on the lower surface of the fuselage. Two tanks are inside the fuselage to load ethanol fuel and LO2. Vehicle design parameters \mathbf{z}_{v} define geometries of the airframe, tanks, and engines as shown in Fig. 2. The intake area of engines and the volume of tanks [V_{ea} and V_{lo} (m³)] are calculated and are passed to other analysis disciplines. Volume efficiency of tanks is 80%, the wing ta-

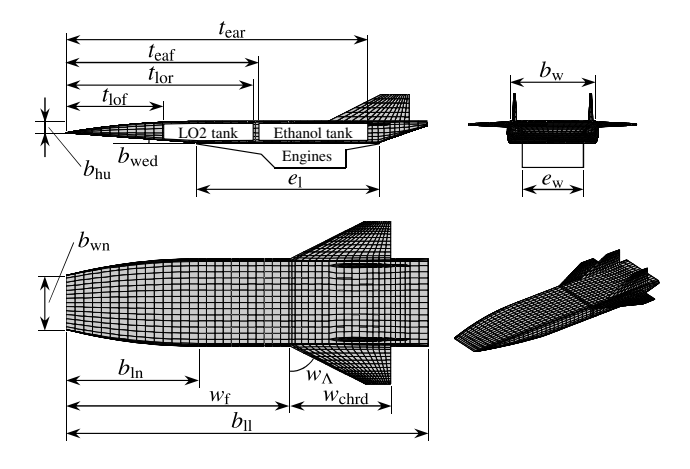


Fig. 2 The configuration and design parameters of the booster.

per ratio is 0.25, and the area of tails is 17 % of the wing area.

Dry mass of the booster $m_{\rm dry}^{\rm boo}$ is computed from $\mathbf{z}_{\rm v}$ and $\mathbf{z}_{\rm a}$. HASA [15], a statistical method for predicting the weight of hypersonic vehicles, is applied to estimate the dry mass excluding engines. The calculation of the engine mass is based on the data provided by JAXA. Consequently, the gross mass of the booster $m_{\rm g}^{\rm boo}$ is

obtained as follows: $m_{\rm g}^{\rm boo} = m_{\rm dry}^{\rm boo} + V_{\rm ea}/729 + V_{\rm lo}/1140$ (kg), where 729 and 1140 are the density of ethanol fuel and LO2 in kg/m³, respectively.

The orbiter has a wave-rider configuration and is loaded on the upper surface of the booster. Design optimization of the orbiter is not conducted in this paper, and its gross mass m_g^{orb} is the constant value, 75 t.

2.3 Aerodynamic Forces

In the aerodynamic analysis, lift force L and drag force D acting on the combined vehicle (booster plus orbiter) are calculated from the airframe geometries and flight conditions in the following manner:

$$\begin{split} L &= q \left\{ S_{\text{ref}}^{\text{boo}}(\mathbf{z}_{\text{v}}) \left[C_{L2}^{\text{boo}}(\mathbf{z}_{\text{v}}, M) \, \alpha^2 \right. \right. \\ &\left. + C_{L1}^{\text{boo}}(\mathbf{z}_{\text{v}}, M) \, \alpha + C_{L0}^{\text{boo}}(\mathbf{z}_{\text{v}}, M) \right] \\ &\left. + S_{\text{ref}}^{\text{orb}} \left[C_{L0}^{\text{orb}}(M) \cos \alpha \right. \right. \\ &\left. - C_{D0}^{\text{orb}}(M) \sin \alpha \right] \right\}, \quad (1) \\ D &= q \left\{ S_{\text{ref}}^{\text{boo}}(\mathbf{z}_{\text{v}}) \left[C_{D2}^{\text{boo}}(\mathbf{z}_{\text{v}}, M) \, \alpha^2 \right. \\ &\left. + C_{D1}^{\text{boo}}(\mathbf{z}_{\text{v}}, M) \, \alpha + C_{D0}^{\text{boo}}(\mathbf{z}_{\text{v}}, M) \right] \right. \\ &\left. + S_{\text{ref}}^{\text{orb}} \left[C_{L0}^{\text{orb}}(M) \sin \alpha \right. \\ &\left. + C_{D0}^{\text{orb}}(M) \cos \alpha \right] \right\}, \quad (2) \end{split}$$

where $S_{\rm ref}^{\rm boo}(\mathbf{z}_{\rm v})$ is the reference are of the booster, and $C_{\rm ref}^{\rm boo}(\mathbf{z}_{\rm v},M)$ is a radial basis function surrogate model [14] of the corresponding aerodynamic coefficient of the booster. Gaussian and thin plate spline are adopted for the basis functions in $\mathbf{z}_{\rm v}$ and M, respectively. As for the orbiter, $S_{\rm ref}^{\rm orb}$, $C_{L0}^{\rm orb}$, and $C_{D0}^{\rm orb}$ are the reference area, the lift coefficient at $\alpha=0$, respectively, which are the constant values provided by JAXA.

In order to train the radial basis function models, an aerodynamic database with different sample values of \mathbf{z}_v and flight conditions is constructed in advance. 200 sample points of \mathbf{z}_v are elaborated using the method proposed in [4] so that they uniformly fill the de-

sign space. For each sample point, aerodynamic forces acting on the booster are calculated in 32 flight conditions (combinations of $M \in \{0.3, 0.6, 1.1, 3.0, 4.0, 7.0, 11.0, 15.0\}$ and $\alpha \in \{0.0, 5.0, 10.0, 15.0\}$ deg). For aerodynamic computations, a program that generates vehicle surface panels is used, and two types of simple CFD methods are applied. For the subsonic or supersonic conditions (M < 2.0), the PAN AIR code [16], a linear potential flow solver using panel methods, is employed. For the hypersonic conditions ($M \ge 2.0$), the tangent cone method [17] and the Prandtl-Meyer expansion flow theory are applied to the impact flow region and the shadow flow region, respectively. Additionally, skin friction is estimated using van Driest's equation [18]. By integrating the pressure coefficient and the friction coefficient over all the panels, aerodynamic forces are obtained.

2.4 Flight Trajectory

For trajectory computations, the 2-DoF vehicle dynamics in the longitudinal plane is employed, and the trajectory prior to the separation of the orbiter is considered. State variables $\mathbf{x}(t)$ include altitude h, velocity v, flight path angle γ , ethanol fuel mass $m_{\rm ea}$, and LO2 mass $m_{\rm lo}$; and control variables $\mathbf{u}(t)$ comprise angle of attack α and throttle τ . State equations are described as follows:

$$\dot{h} = v \sin \gamma, \tag{3}$$

$$\dot{v} = \frac{T\tau\cos\alpha - D}{m} - g\sin\gamma,\tag{4}$$

$$\dot{\gamma} = \frac{T\tau\sin\alpha + L}{m\nu} + \left(\frac{\nu}{h + R_0} - \frac{g}{\nu}\right)\cos\gamma, \quad (5)$$

$$\dot{m_{\rm ea}} = -G_{\rm ea}\tau,\tag{6}$$

$$\dot{m}_{\rm lo} = -G_{\rm lo}\tau,\tag{7}$$

where

$$m = m_{\text{dry}}^{\text{boo}} + m_{\text{ea}} + m_{\text{lo}} + m_{\text{g}}^{\text{orb}}, \tag{8}$$

$$g = g_0 \left(\frac{R_0}{h + R_0}\right)^2. \tag{9}$$

 R_0 (= 6.378 × 10⁶ m) is the mean radius of the Earth, and g_0 (= 9.801 m/s²) is the gravitational

KNOWLEDGE DISCOVERY IN CONCEPTUAL DESIGN OF SPACE PLANES USING MULTI-OBJECTIVE OPTIMIZATION AND DATA MINING

acceleration at the sea level. T, $G_{\rm ea}$, and $G_{\rm lo}$ are calculated in the analysis of the propulsion system; L and D are provided by the analysis of aerodynamic forces; and $m_{\rm dry}^{\rm boo}$ and $m_{\rm g}^{\rm orb}$ are the output from the analysis of vehicle design and dry mass. In order to handle switchovers between engine operating modes, the flight trajectory is divided into three phases to which different modes are assigned: the ejector-jet mode in phase 1 ($t \in [0, t_{\rm ram}]$), the ramjet mode in phase 2 ($t \in [t_{\rm ram}, t_{\rm scram}]$), and the scramjet + rocket mode in phase 3 ($t \in [t_{\rm scram}, t_{\rm f}]$).

The following path constraints are imposed:

$$3 \le M \le 6$$
 for phase 2, (10)
 $-aa_{\text{max}} \le aa \le aa_{\text{max}}$ for all phases, (11)
 $-lf_{\text{max}} \le lf \le lf_{\text{max}}$ for all phases, (12)

$$0 \le q \le q_{\text{max}}$$
 (kPa) for phase 1 & 3, (13)

$$10 \le q \le q_{\text{max}}$$
 (kPa) for phase 2, (14)

$$T\tau \le th_{\text{max}}$$
 (N) for all phases, (15)

where aa and lf are the axial acceleration and the load factor, respectively. Note that aa_{\max} , lf_{\max} , q_{\max} , and th_{\max} are included in \mathbf{z}_a .

A simplified takeoff analysis [19] is conducted assuming that the angle of attack at the takeoff is 15 deg, and the following values are calculated: takeoff speed v_{to} , takeoff length ℓ_{to} , and propellant consumption during the takeoff phase m_{eato} , m_{loto} .

3 Multi-Objective MDO Problem Formulation and Optimization Methodology

Objective functions to be considered include 1) the maximization of the final velocity $v_f := v(t_f)$ (i.e., ΔV attained by the booster), 2) the minimization of the gross mass of the booster m_g^{boo} , and 3) the minimization of the takeoff velocity v_{to} . These objectives are not handled separately but collectively. The multi-objective MDO problem can be formulated as a trajectory optimization problem as follows:

find
$$\mathbf{x}(t)$$
, $\mathbf{u}(t)$, t_{ram} , t_{scram} , t_{f} , \mathbf{z}_{v} , \mathbf{z}_{a} (16) such that min. $F_1 := -v_f$ (m/s),

$$F_2 := m_g^{\text{boo}} \text{ (t)},$$

$$F_3 := v_{\text{to}} \text{ (m/s)}$$
(17)

$$0 \le \alpha \le 15 \text{ deg}, \ 0.1 \le \tau \le 1,$$
 (20)

$$h(0) = 0, \ v(0) = v_{to}, \ \gamma(0) = 0,$$

$$m_{\rm ea}(0) = V_{\rm ea}/729 - m_{\rm eato}$$
 (kg),

$$m_{\rm lo}(0) = V_{\rm lo}/1140 - m_{\rm loto} \,({\rm kg}), \quad (21)$$

$$0 \le t_{\text{ram}} \le t_{\text{scram}} \le t_{\text{f}},\tag{22}$$

$$\ell_{\text{to}} \le 4000 \,\text{m},\tag{23}$$

Additionally, the following bounds are introduced in order to limit the design search space to an interesting area: $v_{\rm f} \geq 3500 \ {\rm m/s}, \ v_{\rm to} \leq 200 \ {\rm m/s}.$

The formulated problem is numerically solved using the method developed in [11]. In this method, a new pareto optimal solution is searched sequentially so that the resulting set of solutions has a good spread in the objective space. This iteration is terminated when the geodesic distance to the nearest solution becomes no more than the user-supplied tolerance d_{tol} for any point on the pareto front. In this paper, let the objective space is defined as $[0.2F_1, 0.1F_2, 2F_3]$, and $d_{tol} = 12.5$. At each iteration, the multi-objective trajectory optimization problem is transformed into a single-objective problem using min-max goal programming [20]. Parameters used in goal programming are determined so that the solution will be located near the farthest point from the solutions obtained so far. Then, dynamic variables [i.e., $\mathbf{x}(t)$ and $\mathbf{u}(t)$] are parameterized, and the trajectory optimization problem is transcribed into a nonlinear programming (NLP) problem via the Legendre-Gauss pseudospectral method [21] with adaptive mesh refinement [22]. \mathbf{z}_t includes these parameterized dynamic variables and $\{t_{\text{ram}}, t_{\text{scram}}, t_{\text{f}}\}$. It should be mentioned that the NLP problem consists of large numbers of design variables and constraints when it becomes a good approximation to the original continuous-time trajectory optimization problem. For solving NLP problems, SNOPT [23], an off-the-shelf solver based on an SQP algorithm, is employed.

The primary advantages of this approach over EAs are as follows:

- 1) The search region of a pareto optimal solution in the objective space can be explicitly specified by the goal-programming parameters, leading to a good spread among solutions regardless of the nonlinearity and convexity of the pareto front.
- 2) Optimization problems with a huge dimensional parameter space and a tiny feasible region can be solved efficiently.
- 3) It is mathematically guaranteed that all the obtained solutions have local pareto optimality within the tolerance of numerical errors.

Numerical models in the MDO problem and the above optimization methodology are implemented in MATLAB® 2007b with some time-consuming components in C++ MEX. Computations are performed on a Windows® 7 machine with an Intel® Core™ i7-4930K CPU and 32 GB RAM.

4 Results and Discussions

4.1 Pareto Optimal Solutions

Figure 3 depicts the obtained 225 solutions in the objective space. Computation time is about 7 hours, which is short enough to handle additional design variables and to adopt more computationally expensive numerical models in the

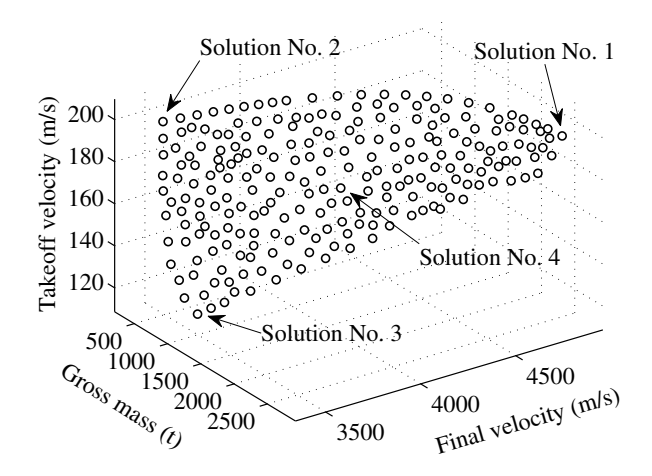


Fig. 3 Obtained 225 solutions in the objective space.

Table 2 Details of the representative solutions.

Domamatan	Unit	Value in solution					
Parameter	Ullit	No. 1	No. 2	No. 3	No. 4		
$v_{ m f}$	m/s	4825.5	3500.0	3500.0	4218.9		
$m_{\rm g}^{ m boo}$	t	2689.6	477.1	997.0	1095.3		
$v_{ m to}$	m/s	200.0	200.0	118.4	161.0		
$m_{ m dry}^{ m boo}$	t	481.3	92.9	229.7	207.6		
$b_{ m ll}$	m	60.0	42.9	60.0	52.6		
$b_{ m w}$	m	24.0	12.5	19.5	17.0		
$b_{ m hu}$	m	2.5	1.2	1.5	1.6		
$b_{ m wed}$	deg	0.0	0.0	0.0	0.0		
$b_{ m ln}$	m	21.6	10.2	10.2	18.3		
$b_{ m wn}$	m	19.2	8.7	8.6	11.7		
$w_{\rm f}$	m	30.0	21.4	30.0	26.3		
$w_{\rm chrd}$	m	24.1	7.3	27.0	19.3		
w_{Λ}	deg	45.0	70.0	45.0	45.4		
$t_{ m lof}$	m	0.0	0.0	0.0	0.0		
$t_{ m lor}$	m	27.7	17.8	18.5	24.5		
$t_{\rm eaf}$	m	28.9	18.7	36.8	25.5		
$t_{\rm ear}$	m	60.0	42.9	60.0	52.6		
e_1	m	30.0	21.6	30.0	26.3		
e_{w}	m	20.0	7.7	10.6	11.1		
aa_{\max}	_	2.7	3.0	2.9	2.7		
lf_{max}	_	1.2	1.3	1.1	1.2		
q_{max}	kPa	50.0	50.0	50.0	50.0		
th_{\max}	MN	23.6	6.5	12.3	11.3		
$M_{\rm ram}^*$	_	3.0	3.0	3.0	3.0		
$M_{\rm scram}^{\dagger}$		5.3	5.5	4.6	5.2		

^{*} Switchover Mach number to ramjet mode.

future work. Note also that all the solutions are nondominated, and they successfully spread uniformly on their underlying surface. The result indicates that three objectives defined in Eq. (17) are conflicting with each other, and all these solutions are optimal from the viewpoint of these design criteria. Table 2 and Figure 4 show details and trajectories of four representative solutions, respectively.

In the solution No. 1, the booster can accelerate up to $v \approx 4800$ m/s whereas its gross mass is excessively large and the takeoff velocity is too high. When the minimization of the gross mass is a primary matter of concern, the optimal booster shape becomes shorter and much slender as shown in the solution No. 2. In order to achieve lower takeoff velocity, it is required to

[†] Switchover Mach number to scramjet + rocket mode.

KNOWLEDGE DISCOVERY IN CONCEPTUAL DESIGN OF SPACE PLANES USING MULTI-OBJECTIVE OPTIMIZATION AND DATA MINING

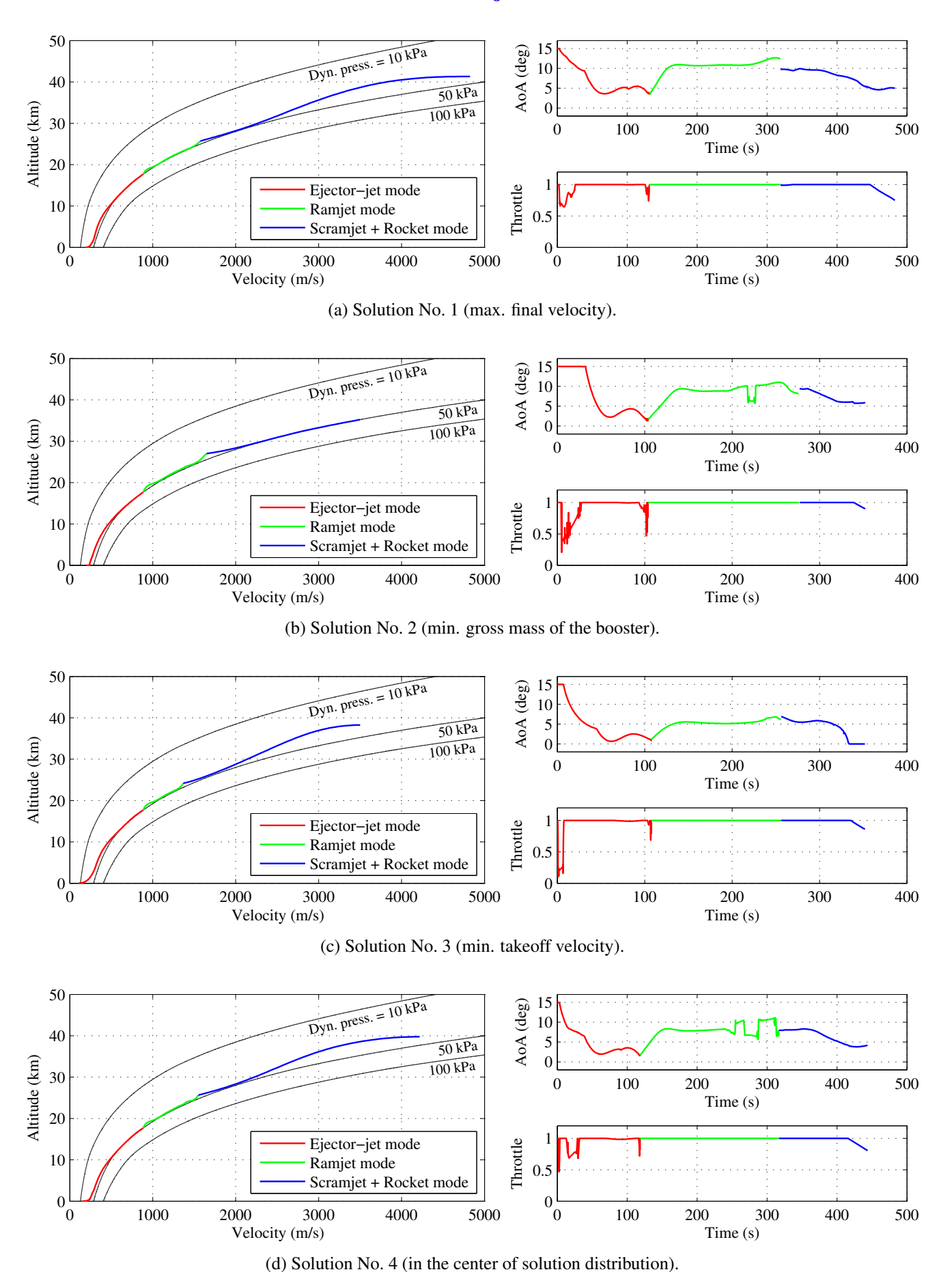


Fig. 4 Flight trajectories of the representative solutions.

load less propellants and make the fuel mass ratio of the booster lower as in the case of the solution No. 3. Vehicle design in the solution No. 4 has intermediate characteristics between that in extreme solutions (i.e., No. 1–3). The optimal $q_{\rm max}$ value is on its upper bound because the performance improvement of engines due to higher $q_{\rm max}$ overcomes the increase of the dry mass calculated by the HASA model. The small $(e_{\rm I}/b_{\rm II})$ value in optimal solutions may result from the exclusion of the scale effect of the RBCC engine performance (larger engines have higher $I_{\rm sp}$).

Since the ramjet mode has higher I_{sp} and lower thrust than the other modes do, the ramjetmode duration occupies from one third to half of the flight while the velocity increment is comparatively small. Before the ascent trajectory smoothly hits the dynamic pressure limit at $h \approx$ 10 km, angle of attack is large, and thrust is throttled. During the flight with the ramjet mode, angle of attack is increased so as to compensate for small thrust. A small deviation from the maximum dynamic pressure around the switchover to the scramjet + rocket mode has an intention to gain more mechanical energy while suppressing the increase of the Mach number. Subsequently to the switchover, dynamic pressure reaches its upper bound again. In the last stage of the trajectory, it is better to fly in lower dynamic pressure and thereby reduce the drag force except the solution No. 2. The reason is that, in these flight conditions, the scramjet has a small contribution compared to the rocket whose performance is independent of dynamic pressure.

4.2 Knowledge Discovery in Solutions

A set of solutions of a multi-objective optimization problem is a large-scale and high-dimensional dataset (i.e., the number of solutions × the number of design variables and objectives therein) and difficult to understand directly. In the previous subsection, four representative solutions were picked out, and some discussions were made on them. In order to extract more general and useful knowledge from all the obtained solutions, data mining techniques are employed [7, 8].

For visualizing the correlation between static variables, a scatter plot matrix can be used. Figure 5 is the scatter plot matrix of objective functions and some parameters. Diagonal elements indicate parameter names, upper-triangular elements depict scatter plots, and lower-triangular elements show Pearson product-moment correlation coefficients. When inspecting the correlation coefficients, note that "correlation does not imply causation". The following information is acquired:

- Maximization of the final velocity is strongly incompatible with the other two objectives. Especially, the gross mass of the booster grows rapidly when the final velocity is desired to be more than 4500 m/s. This implies the necessity of the optimal allocation of velocity increments between the booster and the orbiter.
- Minimization of the booster gross mass and minimization of the takeoff velocity are weakly conflicting with each other. Broadly speaking, parameters that have the considerable correlation with the booster gross mass are not influential on the takeoff velocity a lot.
- It is better to switch to the ramjet mode as soon as possible when it becomes available. Optimal switchover Mach number to the scramjet + rocket mode, on the other hand, spans from 4.6 to 5.6 and is highly associated with the takeoff velocity. When the engines are operated in the ramjet mode for a longer period of time, more ethanol fuel must be loaded, and it leads to larger $(V_{\rm ea}/V_{\rm lo})$ value.
- $(b_{\rm hu}/b_{\rm ll})$ and $(e_{\rm w}/b_{\rm w})$ have a strong positive correlation, indicating that the enlargement of the tanks urged by larger engines is basically accomplished by increasing the fuselage height.

In extracting the underlying structures of dynamic variables, proper orthogonal decomposition (POD) [8] is a powerful tool. In this paper, POD is applied to the time history of angle of attack because it has a significant influence on propulsion and aerodynamics. Using POD, the angle of attack history of the solution No. i $\alpha_i(t)$ is decomposed into that of a nominal solution and

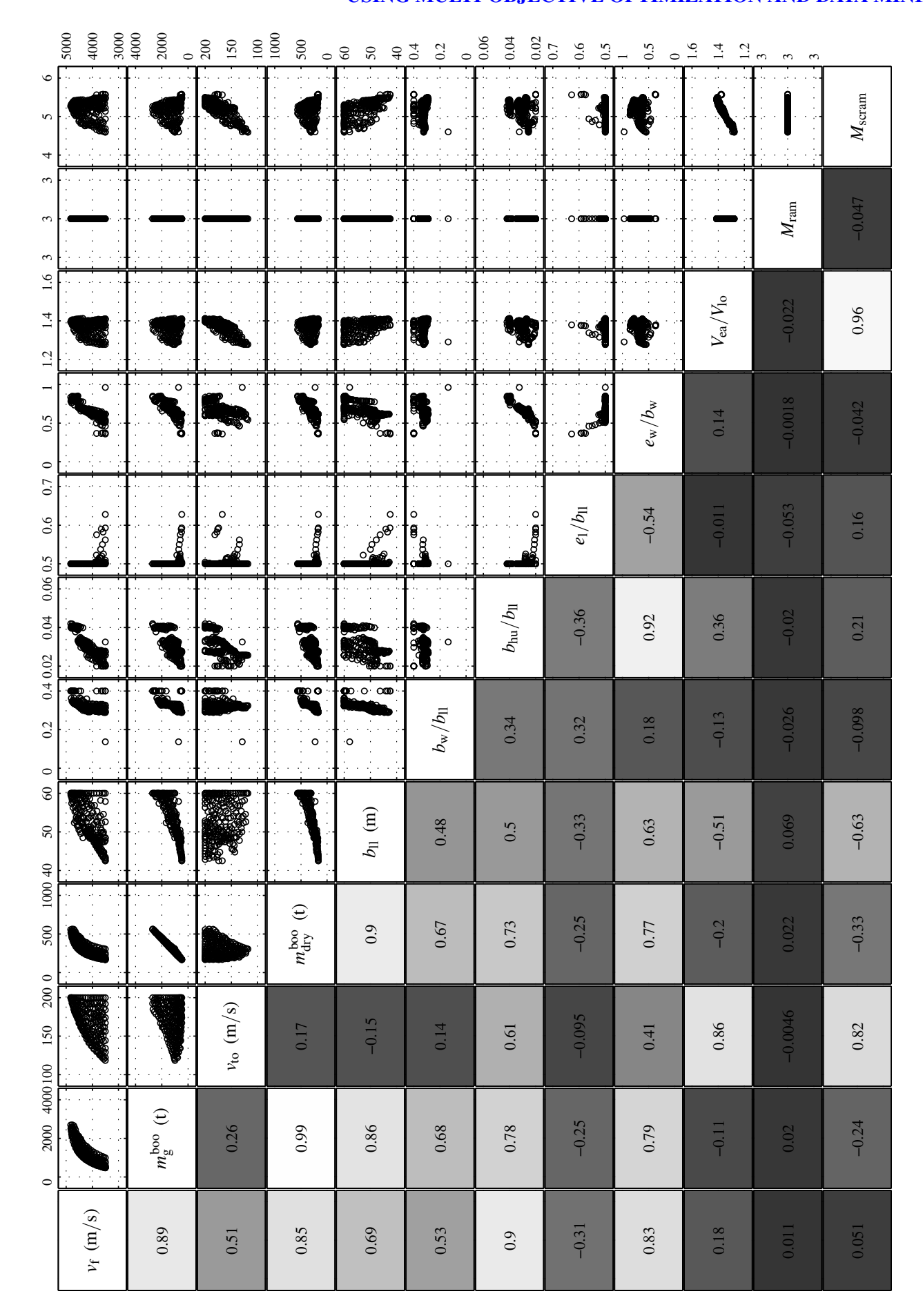


Fig. 5 The scatter plot matrix of the obtained solutions.

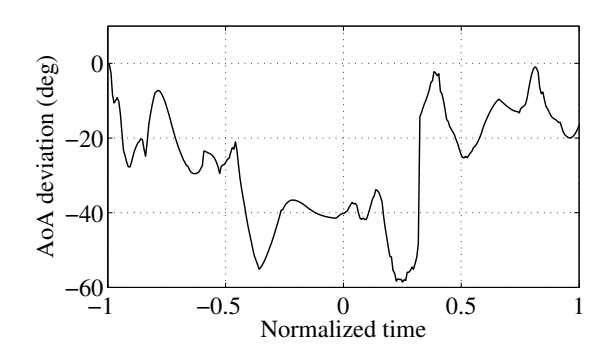


Fig. 6 The dominant basis function $\tilde{\alpha}^{(1)}(\tau)$.

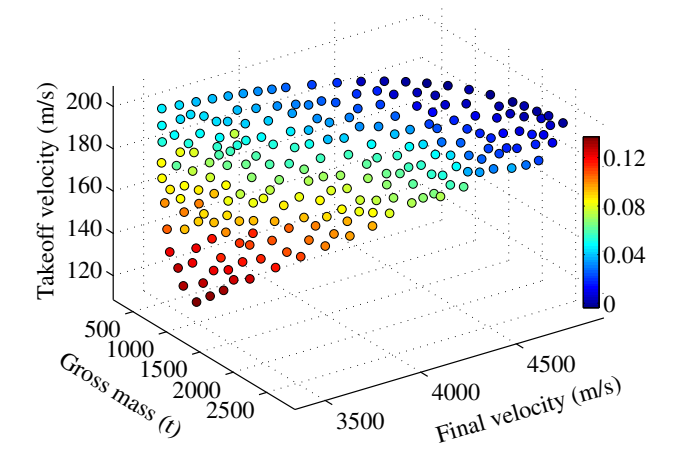


Fig. 7 The coefficients of the dominant mode $a_i^{(1)}$.

the deviation from it:

$$\alpha_i(\tau) = \alpha_1(\tau) + \sum_{j=1}^{225} a_i^{(j)} \cdot \tilde{\alpha}^{(j)}(\tau),$$

$$i = 1, \dots, 225, \quad (25)$$

where the deviation is expressed by the linear combination of basis functions with 225 modes $\{\tilde{\alpha}^{(j)}(\tau), j=1,\ldots,225\}$. The nominal solution (i=1) corresponds to the solution No. 1 discussed in Section 4.1. Due to the optimality of POD, the deviation of each solution from the nominal one can be typically described using a couple of dominant modes. In this case, the most dominant mode (j=1) can express 78.4% of the whole deviation in terms of the energy content. Figures 6 and 7 show its basis function and coefficients, respectively. It is noted that time is normalized from $t \in [0, t_{\rm f}]$ to $\tau \in [-1, 1]$.

The result of POD indicates the following knowledge:

- The coefficients shown in Fig. 7 suggest that the optimal time history of angle of attack during the flight relies primary on the takeoff velocity and slightly on the final velocity. When the lower takeoff velocity is desired and/or the final velocity is not required to be so high, the optimal angle of attack becomes smaller (the basis function whose coefficients get larger has a negative value throughout its domain). This tendency can be attributed to the fact that the optimal booster design in this kind of situation has lower wing loading.
- The dominant basis function has a larger negative value in $\tau \in [-0.4, 0.3]$ compared to the other region. This means that the sensitivity of the optimal angle of attack during the ramjet mode to the design preference is high.

5 Conclusion

In this paper, a multi-objective, multidisciplinary conceptual design study of the booster of a horizontal takeoff and landing TSTO space plane with RBCC engines was performed. The MDO framework that handles the interdependence between flight trajectories, propulsion, vehicle geometries, and aerodynamics was constructed, and the multi-objective MDO problem was formulated with the following objective functions: the maximization of the final velocity, the minimization of the booster gross mass, and the minimization of the takeoff velocity. A set of pareto optimal solutions exhibiting the trade-off relation among these design criteria was obtained using a newly developed multi-objective optimization methodology. After some discussions were made on four selected solutions, correlation analyses of the pareto optimal solutions were conducted via two data mining techniques (a scatter plot matrix and POD). This paper revealed some knowledge on the optimal design of the booster and its trajectory, and demonstrated the applicability of the novel optimization method to multi-objective MDO problems.

In the future work, the following improvements in the accuracy of numerical models are indispensable for acquiring more reliable and insightful design knowledge: applying higher fi-

KNOWLEDGE DISCOVERY IN CONCEPTUAL DESIGN OF SPACE PLANES USING MULTI-OBJECTIVE OPTIMIZATION AND DATA MINING

delity models to the estimation of vehicle mass and aerodynamic forces; including the scale effect of the engine performance; taking the interaction between airframe and propulsion into consideration; and considering rigid body characteristics of the vehicle. Besides, optimization of the overall TSTO system including the orbiter design and the flight trajectory after the separation of the orbiter will be conducted.

6 Acknowledgements

This study was conducted as a collaborative research with Japan Aerospace Exploration Agency (JAXA). The author would like to thank Dr. Tomioka of JAXA for providing data on RBCC engines and the orbiter vehicle.

7 Contact Author Email Address

mailto: 2479128814@mail.ecc.u-tokyo.ac.jp

References

- [1] Yoshida M, Ishimoto S, Kimura T, Tomioka S, Kodera M, and Tani K. Future space transportation vehicle study at JAXA. *Proc. of the 63rd International Astronautical Congress*, Naples, Italy, Oct. 2012.
- [2] Kodera M, Ogawa H, Tomioka S, and Ueda S. Multi-objective design and trajectory optimization of space transportation systems with RBCC propulsion via evolutionary algorithms and pseudospectral methods. *Proc. of the AIAA SciTech*, Maryland, USA, Jan. 2014.
- [3] Tsuchiya T and Mori T. Optimal design of two-stage-to-orbit space planes with airbreathing engines. *Journal of Spacecraft and Rockets*, Vol. 42, No. 1, pp. 90–97, 2005.
- [4] Yokoyama N, Suzuki S, Tsuchiya T, Taguchi H, and Kanda T. Multidisciplinary design optimization of space plane considering rigid body characteristics. *Journal of Spacecraft and Rockets*, Vol. 44, No. 1, pp. 121–131, 2007.
- [5] Tsuchiya T, Takenaka Y, and Taguchi H. Multidisciplinary design optimization for hypersonic experimental vehicle. *AIAA Journal*, Vol. 45, No. 7, pp. 1655–1662, 2007.
- [6] Betts J. Practical methods for optimal control

- and estimation using nonlinear programming. SIAM, 2001.
- [7] Jeong S, Chiba K, and Obayashi S. Data mining for aerodynamic design space. *Journal of Aerospace Computing, Information, and Communication*, Vol. 2, No. 11, pp. 452–469, 2005.
- [8] Oyama A, Nonomura T, and Fujii K. Data mining of pareto-optimal transonic airfoil shapes using proper orthogonal decomposition. *Journal of Aircraft*, Vol. 47, No. 5, pp. 1756–1762, 2010.
- [9] Deb K. Multi-objective genetic algorithms: Problem difficulties and construction of test problems. *Evolutionary Computation*, Vol. 7, No. 3, pp. 205–230, 1999.
- [10] Iorio A and Li X. Rotated problems and rotationally invariant crossover in evolutionary multiobjective optimization. *International Journal of Computational Intelligence and Applications*, Vol. 7, No. 2, pp. 1–38, 2008.
- [11] Fujikawa T and Tsuchiya T. Multi-objective, high-accuracy trajectory optimization using SQP and sampling on the manifold. *Proc. of the 2013 Asia-Pacific International Symposium on Aerospace Technology*, Takamatsu, Japan, Nov. 2013.
- [12] Kanda T, Tani K, and Kudo K. Conceptual study of a rocket-ramjet combined-cycle engine for an aerospace plane. *Journal of Propulsion and Power*, Vol. 23, No. 2, pp. 301–309, 2007.
- [13] Tomioka S, Hiraiwa T, Saito T, Kato K, Kodera M, and Tani K. System analysis of a hydrocarbon-fueled RBCC engine applied to a TSTO launch vehicle. *Proc. of the 29th International Symposium on Space Technology and Sciences*, Nagoya, Japan, June 2013.
- [14] Forrester A, Sóbester A, and Keane A. Engineering design via surrogate modelling: A practical guide. John Wiley & Sons, 2008.
- [15] Harloff G and Berkowitz B. HASA: Hypersonic aerospace sizing analysis for preliminary design of aerospace vehicles. NASA CR-182226, 1988.
- [16] Epton M and Magnus A. PAN AIR: A computer program for predicting subsonic linear potential flows about arbitrary configurations using a higher order panel methods, Vol. 1: Theory document. NASA CR-3251, 1991.
- [17] Pittman J. Application of supersonic linear theory and hypersonic impact methods to three nonslender hypersonic airplane concepts at Mach

- numbers from 1.10 to 2.86. NASA TP-1539, 1979.
- [18] White F. *Viscous fluid flow*. McGraw-Hill, pp. 550–551, 1991.
- [19] Raymer D. Aircraft design: A conceptual approach. AIAA, pp. 563–566, 1999.
- [20] Miettinen K. Nonlinear multiobjective optimization. Kluwer. 1999.
- [21] Benson D, Huntington G, Thorvaldsen T, and Rao A. Direct trajectory optimization and costate estimation via an orthogonal collocation method. *Journal of Guidance, Control, and Dynamics*, Vol. 29, No. 6, pp. 1435–1440, 2006.
- [22] Fujikawa T and Tsuchiya T. Enhanced mesh refinement in numerical optimal control using pseudospectral methods. *SICE Journal of Control, Measurement, and System Integration*, Vol. 7, No. 3, pp. 159–167, 2014.
- [23] Gill P, Murray W, and Saunders M. SNOPT: An SQP algorithm for large-scale constrained optimization. *SIAM Review*, Vol. 47, No. 1, pp. 99–131, 2005.

Copyright Statement

The authors confirm that they, and/or their company or organization, hold copyright on all of the original material included in this paper. The authors also confirm that they have obtained permission, from the copyright holder of any third party material included in this paper, to publish it as part of their paper. The authors confirm that they give permission, or have obtained permission from the copyright holder of this paper, for the publication and distribution of this paper as part of the ICAS 2014 proceedings or as individual off-prints from the proceedings.